nature communications

Article

https://doi.org/10.1038/s41467-025-58191-w

Deformation resistant monolithic hierarchical textures inducing stretchable superamphiphobicity with environmental adaptability and flame retardancy

Received: 18 November 2024

Accepted: 13 March 2025

Chun-Bo Li[1], Fang Wang[1,2] ✉, Yi-Yang Wang[1], Mei-Lin Guo[1], Jin-Le Li[1], Cong Deng[1], Fei Song[1], Wei Yang[2] & Yu-Zhong Wang[1] ✉

Superamphiphobic and flame-retardant fabrics offer effective protection for firefighters and industrial workers operating under hazardous conditions. However, limitations in deformation resistance, wear comfort, and environmental adaptability hinder their practical applications. Here, a monolithic hierarchical macro-/micro-/nanostructure is constructed to achieve durable repellency against water and oils, even under significant deformations. This coating integrates fluorinated nanoparticles, flame retardant microparticles, and a cross-linking adhesive. Hydrogen bonding and the adhesive define the coating's morphology, robustness, and adaptability. The coated surface exhibits an ultralow water adhesion force (0.002 mN) and excellent anti-fouling performance against extreme temperatures (100 °C, −196 °C) and corrosive liquids, including aqua regia and concentrated H_2SO_4. Upon fire exposure, the coating enables self-extinguishing behavior on cotton fabrics. The coated fabrics also demonstrate remarkable mechanical and UV resistance while preserving wear comfort. Overall, we achieve a balance between desirable properties and wear comfort in superamphiphobic, flame-retardant fabrics, enabling protective clothing applications previously unattainable.

Clothing serves as a crucial second skin, offering both comfort and protection across diverse environments. Fabrics possessing flexibility and breathability are one of the most pivotal clothing materials, providing great convenience in industrial production and daily life[1]. These fabrics primarily comprise natural fibers such as cotton, silk, and linen, as well as synthetic fibers like polyester, nylon, and polypropylene[2]. However, when used in personal protective textiles for industrial workers and firefighters in hazardous conditions, several challenges arise: (1) the vast majority of fabrics are highly susceptible to rapid ignition upon exposure to fire, increasing the risks of fire hazards during use[3,4]; (2) fabrics are prone to contamination from water and oil, leading to appearance defects and performance degradation; (3) the growing demand for diverse applications requires fabrics to withstand harsh environments, including UV radiation, chemical corrosion, high temperatures, and freezing conditions[5,6]. To address these issues, many efforts, such as physical blending[7], chemical grafting[8], organic/inorganic hybrid coating[9–12], and sol-gel reactions[13], have been explored to enhance fabrics' flame retardancy, hydrophobicity, and oleophobicity. The incorporation of flame-retardant elements, including halogens, phosphorus, nitrogen, silicon, and boron, has been shown to be effective in enhancing fire safety. However, the high sensitivity of these components to moisture often leads to their

---

[1]The Collaborative Innovation Center for Eco-Friendly and Fire-Safety Polymeric Materials (MoE), National Engineering Laboratory of Eco-Friendly Polymeric Materials (Sichuan), National Key Laboratory of Advanced Polymer Materials, College of Chemistry, Sichuan University, Chengdu 610064, China. [2]College of Polymer Science and Engineering, Sichuan University, Chengdu 610064, China. ✉e-mail: wangfang99@scu.edu.cn; yzwang@scu.edu.cn

migration and failure, especially in humid environments or after repeated washing, which significantly limits their practical application[14].

To fight against the leaching of flame retardants, integrating superhydrophobicity with flame retardancy provides a promising solution. Various materials, such as polydimethylsiloxane-silica/ammonium polyphosphate (APP) hybrid coatings[15–18], phytic acid metal complex aggregations/dimethyloctadecyl [3-(trimethoxysilyl) propyl] ammonium chloride hybrid coatings[19], hydroxyethyl acrylate/sodium vinylsulfonate copolymers[20], and ethylene-vinyl acetate/aluminum trihydroxide composite[21], have demonstrated the feasibility of this strategy. However, superhydrophobicity alone is insufficient to prevent appearance defects or reduce the increased fire risk caused by oil contamination (e.g., edible oil, diesel) on flame-retardant materials, particularly under hazardous conditions.

Compared to superhydrophobic materials, superamphiphobic surfaces provide superior oil repellency and enhanced anti-fouling performance[22]. Over the past decade, many methods, such as laser-etching[23], template-assisted electrochemical deposition, 3D-printing technologies, and inorganic/organic hybrid coating[24–30], have been proposed to create superamphiphobic surfaces. However, sophisticated fabrication processes often hinder their practical application, making scalable, easy-to-manufacture coatings the preferred solution[31,32]. By optimizing the composition, size, and parameters of the inorganic/organic components, the properties of coated fabrics can be significantly improved[33,34]. Despite these advancements, it remains a daunting challenge to maintain superamphiphobicity under harsh external environments such as long-term mechanical abrasion or large deformations[35–43]. In addition, personal protective clothing requires resistance to extreme acid/base corrosion, UV irradiation, and hot/cold liquids, while also ensuring wear comfort (e.g., water moisture/air permeability and bending rigidity)[44]. Unfortunately, so far, there exists a glaring gap in achieving the integration of these functions within one material with well-balanced performance.

In this work, a distinctive scalable coating with integrated superamphiphobicity and flame retardancy for functional fabrics used in personal protective clothing is presented. Attributed to the well-arranged fluorinated silica (F-SiO_2) nanoparticles, micro-sized aluminum diethylphosphinate (ADP) particles and cross-linking polydimethylsiloxane (PDMS) adhesive, the obtained coating exhibits super-repellency to both water and oils, even under significant deformations. The inorganic functional micro/nanoparticles provide optimal multi-scale roughness and generate a monolithic hierarchical macro-/micro-/nanostructure with substrates, endowing the surfaces with impressive air trap capability. The trapped air cushion imparts durable repellency to hot (100 °C), cold (−196 °C), and corrosive liquids (even aqua regia and concentrated H_2SO_4). The coated surface achieves an ultralow water adhesion force as low as 0.002 mN. The combined efforts of hydrogen bonding interactions and cross-linking elastic adhesive enhance the coating's mechanical robustness, and environmental adaptability, such as UV resistance, and corrosion resistance, while maintaining excellent water moisture permeability, bending rigidity, and tensile strength. More importantly, applying the coating to cotton fabric imparts self-extinguishing behavior in the vertical burning test. This multifunctional, superamphiphobic, and flame-retardant material demonstrates significant potential for advanced functional textiles and personal protective clothing applications.

Results

Physicochemical characterization of the SFC coating

A schematic diagram depicting the preparation process of superamphiphobic and flame-retardant coating (SFC) is illustrated in Fig. 1. Due to the strong hydrogen bonding interactions and the cross-linking capability of the PDMS adhesive, F-SiO_2 integrates with ADP to form micro-nano aggregates, thereby creating a monolithic hierarchical macro-/micro-/nanostructure on the substrates. In addition, quite low surface energy is a critical factor in preventing surfaces from being wetted by liquids with low surface tensions, such as edible oil (33 mN m^{-1}) and concentrated H_2SO_4 (55 mN m^{-1}). 1H,1H,2H,2H-Perfluorodecyltriethoxysilane (PFDTES) is utilized to lower the surface energy of the micro-nano aggregates. The coated surfaces exhibit excellent air-trapping capabilities, forming distinct bright and light-reflecting silver mirrors even in challenging environments such as boiling water, ice water, and 98% H_2SO_4 (Supplementary Fig. 1). The components of the superamphiphobic coating are systematically optimized to balance superamphiphobicity, flame retardancy and mechanical stability, resulting in superior comprehensive performance compared to previously reported materials (Supplementary Fig. 2 and Supplementary Table 1).

The surface morphologies of coatings with varying ratios (r) are presented in the scanning electron microscopy (SEM) images (Fig. 2a and Supplementary Fig. 3). When $r = 0$, the coating appears relatively smooth without any observable micro-nanostructures. As r increases to 0.5, micro-protuberances begin to emerge due to the encapsulation of micro-nano aggregates by PDMS. Notably, when $r > 0.8$, a unique hierarchical surface structure is formed, characterized by densely packed nanoparticles and abundant micro-protuberances (~0.5–10.0 μm). Cross-sectional SEM images (Supplementary Fig. 4) reveal a similar structure, with the overall coating thickness measuring approximately 118 μm.

To gain a deeper understanding of the interactions of the SFC coating, molecular electrostatic potential (ESP) maps are generated to visualize the electron distribution patterns (Supplementary Figs. 5 and 6), thereby enabling a detailed analysis of the regions characterized by hydrogen bonding. The positively charged regions (highlighted in red) are primarily located on the hydroxyl and alkyl groups, while the negatively charged regions (in blue) are concentrated on the oxygen and fluorine atoms, illustrating the possible formation regions of hydrogen bonds (Fig. 2b). In addition, the interaction conformations of a three-molecule cluster are explored using molecular dynamic annealing (Supplementary Fig. 7). The most stable conformation, presented in Fig. 2c, exhibits a calculated binding energy of −73.9 kcal mol^{-1}, indicating a significant decrease in the total system energy. This reduction in energy suggests the formation of a more stable assembled structure[45].

Temperature-dependent Fourier transform infrared spectroscopy (FTIR) spectra and 2D correlation FTIR spectra are employed to investigate the interactions among the functional groups in the SFC coating. Upon heating from 30 to 210 °C, the -OH stretching band near 3410 cm^{-1} undergoes a noticeable blue shift, along with a significant decrease in intensity (Fig. 2d). Similarly, blue shifts and intensity reductions are observed for the Si–O–Si stretching band at 1080 cm^{-1}, the P=O stretching band at 1150 cm^{-1}, and the $-CF_2$ stretching band at 1230 cm^{-1}, indicating the disruption of hydrogen bonds involving these groups. The synchronous and asynchronous spectra (Fig. 2e and Supplementary Fig. 8) confirm the existence of different types of hydrogen bonds within the SFC coating[46]. The FTIR, X-ray photoelectron spectroscopy (XPS) spectra and elemental mapping results indicate a homogeneous deposition of the coating onto the substrates (Fig. 2f–h, Supplementary Figs. 9 and 10, and Supplementary Note 1).

Surface wettability

To explore the effect of surface roughness on wettability, the contact angles (CAs) and sliding angles (SAs) of water and edible oil on surfaces with varying r values are determined (Fig. 3a and Supplementary Fig. 11), corresponding to the schematic in Fig. 3b. At low r values ($r \leq 0.3$), the surfaces exhibit relatively hydrophobic and oleophilic properties, due to the smooth morphology and low roughness. As the r value increases to a medium range ($0.4 \leq r \leq 0.6$), the wettability

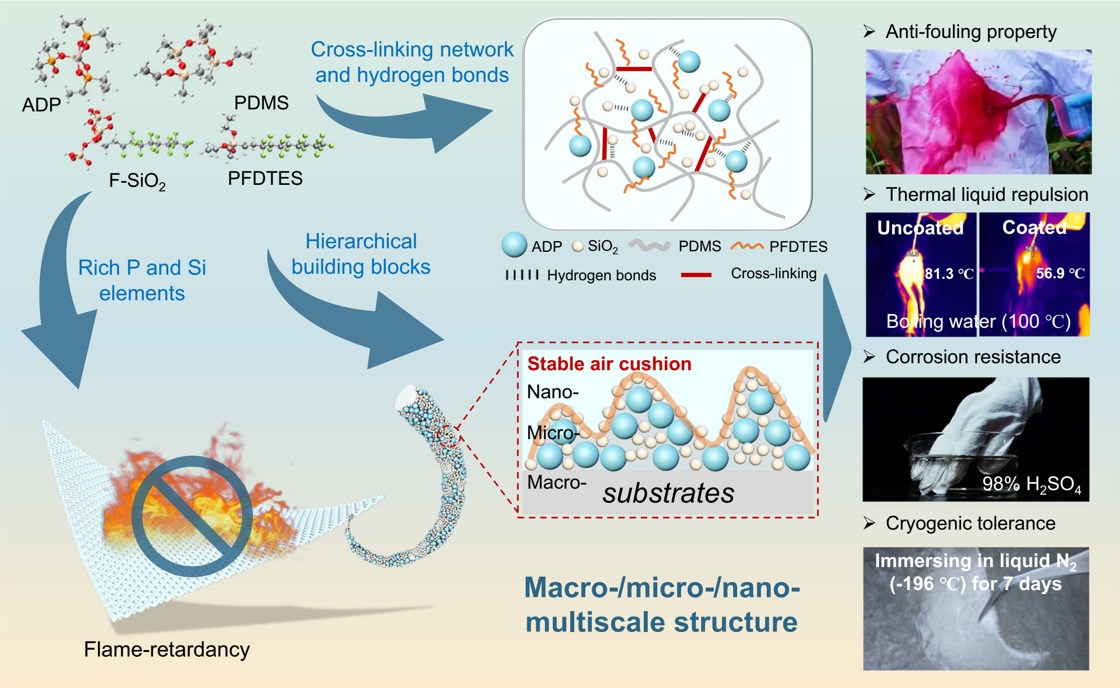

Fig. 1 | Schematic representation of the preparation of the SFC coating. Schematic illustration detailing the fabrication process and applications of the SFC coating.

of the samples transforms to superhydrophobic/oleophobic, facilitated by the formation of microstructures and increased surface roughness. Further increasing the r value ($0.7 \le r \le 1.0$) leads to a transition to superamphiphobicity, where both water and edible oil display CAs exceeding 150°, indicating the formation of a micro-nano rough structure. Thus, by tuning the r values, the surface wettability can be controlled. A relatively high surface roughness of 4.92 µm is recorded at $r = 0.8$ (Fig. 3c and Supplementary Fig. 12). In addition, the effects of different F-SiO$_2$ to ADP ratios on both anti-wetting properties and flame retardancy have been evaluated (Supplementary Figs. 13 and 14, and Supplementary Note 2). Considering the need for balanced performance, the sample with $r = 0.8$ and F-SiO$_2$:ADP = 5:5 was selected for further investigation.

In addition to water and edible oil droplets, various common liquids can keep spherical shape on the surface of coated fabric, with CAs exceeding 150° (Fig. 3d). In contrast, these liquid droplets instantly permeate the uncoated fabric when touching the surface (Supplementary Fig. 15). Furthermore, substrates such as cotton fabric, filter paper, spandex, and foam can be uniformly modified with the SFC coating and exhibit super-repellency to both water and edible oils (Supplementary Figs. 16 and 17). Figure 3e further illustrates that all the coated substrates show bright and light-reflecting surfaces underwater, acting like silver mirrors, which confirms the presence of air cushions captured by the surface's rough texture.

All the coated substrates exhibit an ultralow water adhesion force below 0.011 mN, with narrow peaks indicating rapid detachment of the water droplet from the coated substrates (Fig. 3f and Supplementary Fig. 18). In contrast, the uncoated surfaces show significantly higher adhesion forces, ranging from 0.169 to 0.410 mN, with residual water left behind upon droplet removal. The ultralow adhesion force can be attributed to the low surface energy, the unique monolithic hierarchical macro-/micro-/nanostructure, and the presence of trapped air cushions.

The drop impact experiment (Fig. 3g) displays that a water droplet can bounce freely off the surface multiple times without leaving any residual, illustrating the excellent surface robustness. Figure 3h records the dynamic wetting behaviors of water and edible oil droplets on the coated cotton fabric. Despite partial evaporation, the droplets maintain their spherical shape, and the surface preserves its anti-wetting state for 60 min, suggesting the high stability of the superamphiphobicity of the coated cotton fabrics.

Antifouling, thermal, cryogenic, and chemical resistances

With increasing concerns for the safety of industrial workers exposed to harsh weather and hazardous conditions, protective clothing is extremely important to people's lives. Thanks to the ultralow water adhesion force, the coated cotton fabrics exhibit excellent anti-fouling performance. Continuous water droplets can carry away FeCl$_3$ particles easily from the coated cotton fabric at a slight titling angle of 15° (Fig. 4a). Supplementary Fig. 19 shows that the coated glove remains clean and dry, even after immersing or stirring in muddy water. Contaminated liquids could readily bounce off the coated protective clothing, leaving it moisture-free and spotless (Fig. 4b). Moreover, in practical usage scenarios, holding and lifting heavy objects do not significantly affect the superamphiphobicity of the coated gloves and protective clothing (Supplementary Figs. 20 and 21).

Enhancing personal protective equipment with thermal protection is crucial for reducing the risk of scalding[47,48]. We employ an infrared (IR) camera to record the process of pouring 100 mL of boiling water onto both uncoated and coated gloves. The uncoated glove is immediately wetted upon contact with the boiling water, causing the surface temperature sharply increase to ~81 °C (Fig. 4c). After 5 s, the temperature is remained at ~61 °C (set the end time of hot water shock as 0 s), potentially leading to scalding. In contrast, boiling water did not penetrate the coated glove but slide off without any adhesion. The surface temperature rapidly drops from ~52 °C to ~38 °C after 5 s, which is attributed to the presence of the enough air pockets trapped in the surface's micro-nanostructure, and hence to efficiently reduce the contact area and retention time of hot water.

To investigate the resistance of the SFC coating against harsh chemical corrosions, the coated cotton gloves against concentrated H$_2$SO$_4$ (98%) are tested. The uncoated cotton glove immediately suffers severe corrosion and damage upon immersing in the concentrated H$_2$SO$_4$, resulting in injury to the artificial hand (Fig. 4e). However, due

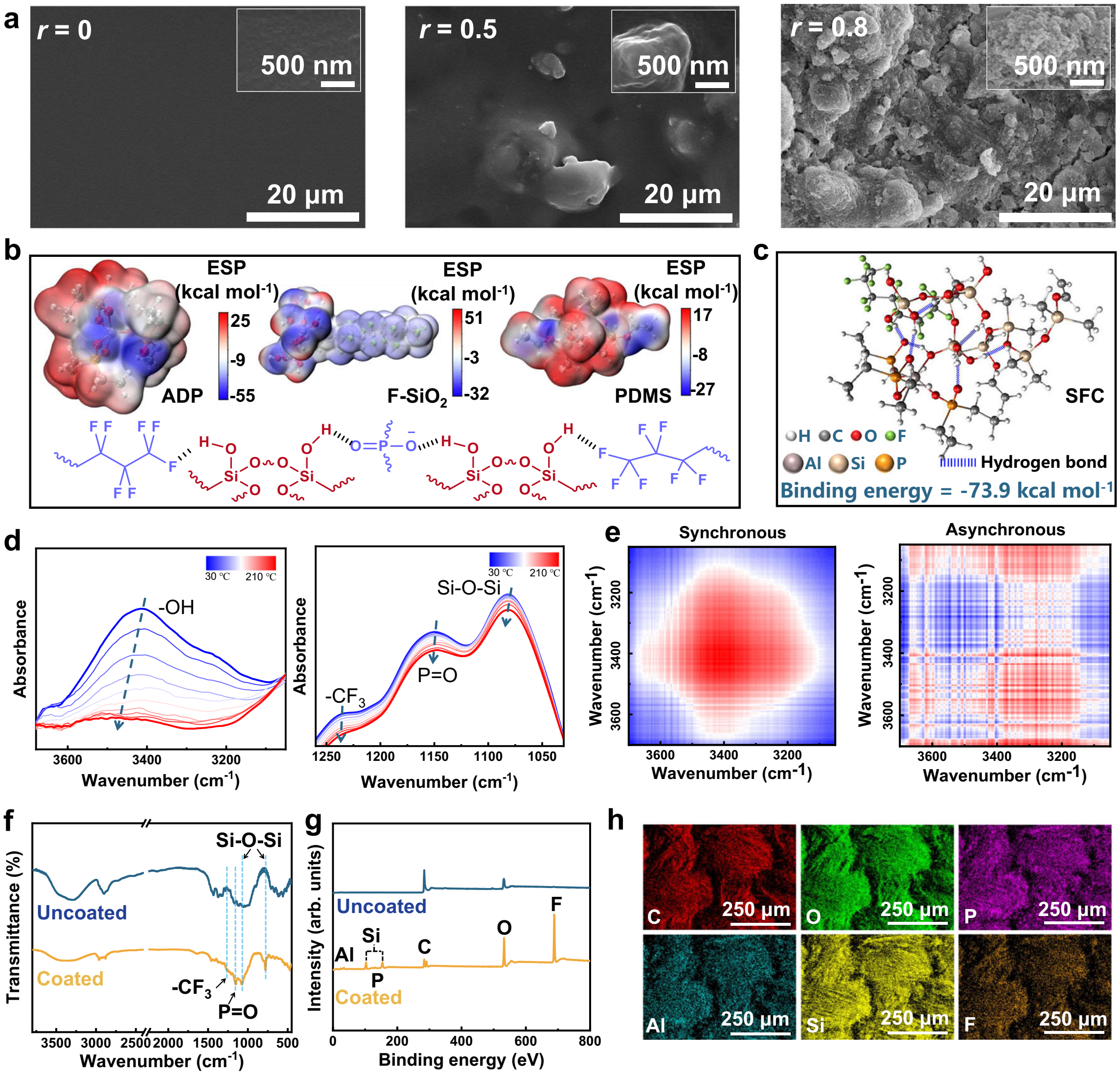

Fig. 2 | Surface morphologies and structural characterization. a SEM images of the as-prepared coating surface at various *r* values [$r = (W_{F\text{-}SiO2} + W_{ADP})/(W_{F\text{-}SiO2} + W_{ADP} + W_{PDMS})$]. The insets show higher magnification SEM images. **b** Molecular electrostatic potential (ESP) plots for ADP, F-SiO_2, and PDMS, respectively. **c** Binding energy calculations for the conformational interactions within the three-molecule cluster. **d** Temperature-dependent FTIR spectra of the SFC coating upon heating from 30 °C to 210 °C. The arrows denote the direction of the corresponding peak shifts. **e** Synchronous and asynchronous 2D correlation FTIR spectra of the SFC coating. Red colors are defined as positive intensities, while blue colors are defined as negative ones. **f**, **g** FTIR spectra (**f**) and XPS (**g**) survey spectra of uncoated and coated cotton fabrics. **h** EDS elemental mapping analysis of the SFC-coated cotton fabric.

to the existence of the air cushion, as evidenced by the silver mirror phenomenon shown in Fig. 4e, the coated glove can effectively resist the wetting of the concentrated H_2SO_4 and protect the hand from erosion. In addition, the superamphiphobic coating retains its liquid repellency after 168 h of exposure to seawater, dimethyl sulfoxide (DMSO), N, N-dimethylformamide (DMF), aqua regia, concentrated H_2SO_4 (98%), and NaOH solution (pH = 14) (Fig. 4d and Supplementary Fig 22), with the hierarchical micro-/nanostructures are preserved (Supplementary Fig. 23). The good chemical stability is attributed to the hydrogen bonding interactions, high cross-linking of the PDMS adhesive, appropriate surface roughness, and the ultra-low surface energy of PFDTES.

To assess the resistance of the coated fabric against harsh cold environments, the icing process of water droplets on different surfaces is observed. Due to the hydrophilicity of the uncoated cotton fabric, the water droplet quickly spreads on the surface (Fig. 4f). For the commercial chemical and firefighting protective clothing (control sample 1 and sample 2), ice formation at 150 s and 231 s, respectively (Supplementary Figs. 24 and 25), marks the termination of the icing process. In contrast, the coated fabric exhibits a freezing delay time of 1613 s, which is nearly 50 times longer than that of the uncoated fabric. Temperature-time curves and IR images (Fig. 4g and Supplementary Figs. 26 and 27) reveal that the SFC-coated fabric can prolong the cooling time (42 s, the time required for the water temperature to drop to 0 °C) and icing time (327 s, the time from the onset of icing to the complete solidification of the water). Furthermore, the ice adhesion strength of the SFC-coated fabric is only 2.8 ± 0.6 kPa, significantly lower than other samples (Fig. 4h). The good anti-icing performance originates from the existence of stable thermally insulating air cushions, which effectively reduces heat transfer between the water droplets and the fabric.

The COMSOL simulation results in Fig. 4j and Supplementary Fig. 28 illustrate the phase change and freezing process. These simulated results are consistent with the experimental data on delayed freezing, further confirming the excellent anti-icing properties of the SFC-coated fabrics[49]. Moreover, after pouring 50 mL of liquid N_2 on the

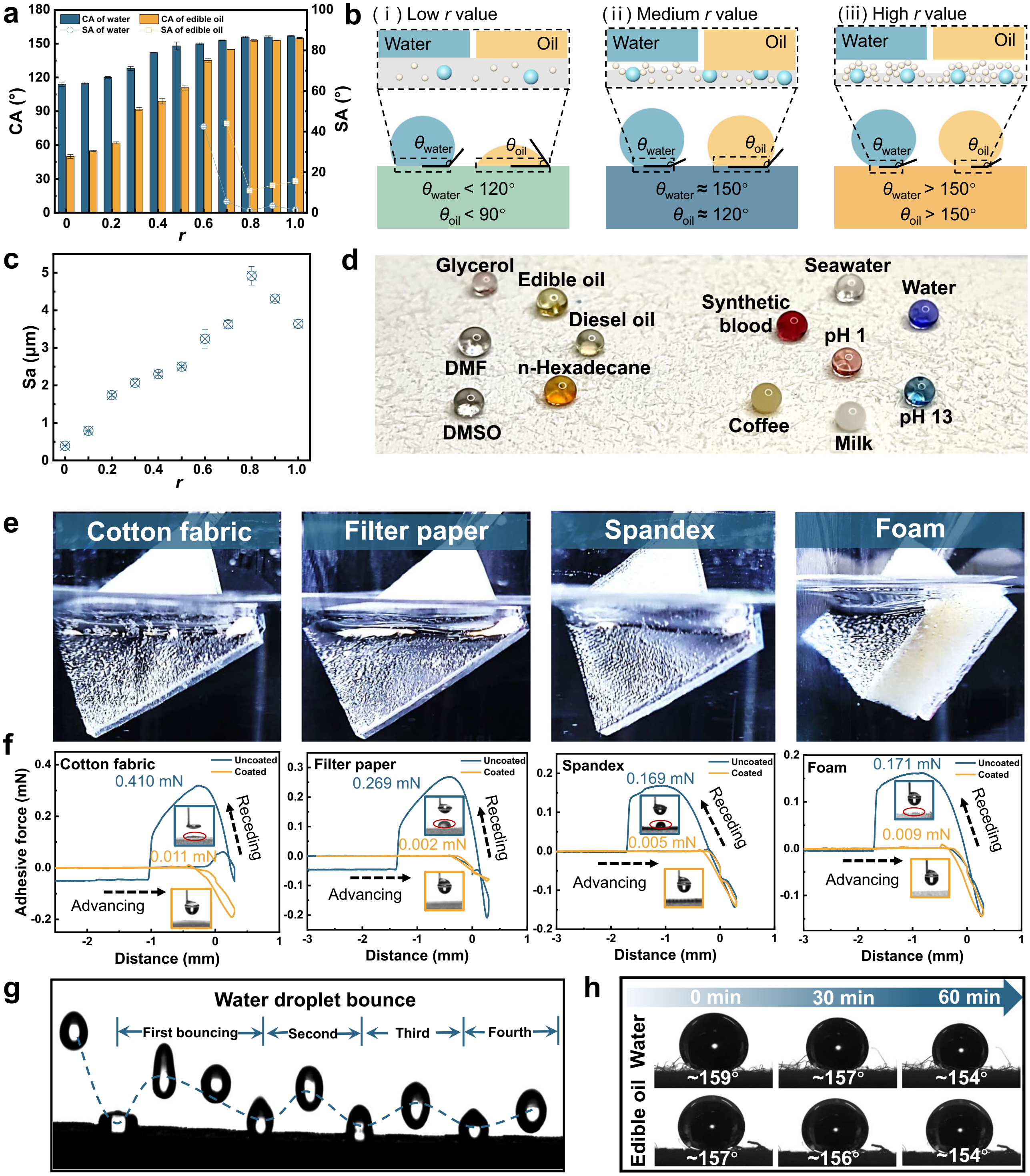

Fig. 3 | Surface wettability. a Contact angles (CAs) and sliding angles (SAs) of water and edible oil on the as-prepared coating surfaces at different *r* values. **b** Schematic illustration of liquid-wetting models for the coating surfaces. **c** Relative surface roughness of the as-prepared coating surfaces at different *r* values. **d** Digital photographs showing the wettability of various liquids on coated cotton fabric. **e** Digital photographs of coated substrates (including cotton fabric, filter paper, spandex, and foam) immersed in water, exhibiting a silver mirror-like phenomenon. **f** The corresponding water adhesion force of the uncoated and coated substrates. **g** A sequence of graphs recorded a water droplet (10 μL) impacting and bouncing on the coating surface (droplet release height: 2 cm). **h** Optical images of water and edible oil droplets placed on the coated cotton fabric as a function of testing time (environment temperature: 20 °C; relative humidity: 65%). All error bars represent the standard deviations calculated from at least three independent measurements. Source data are provided in the Source data file.

SFC-coated fabric or immersing it in liquid N_2 (−196 °C) for 7 days, the fabric retains its superamphiphobicity when returned to ambient temperature (Fig. 4i and Supplementary Fig. 29). This demonstrates the coating's satisfactory cryogenic environment tolerance.

Imparting flame retardancy to fabrics is particularly important in scenarios such as chemical production and indoor furnishings. After being exposed to a direct flame for 12 s, the uncoated cotton fabric and commercial control sample 1 ignited immediately, leaving little char

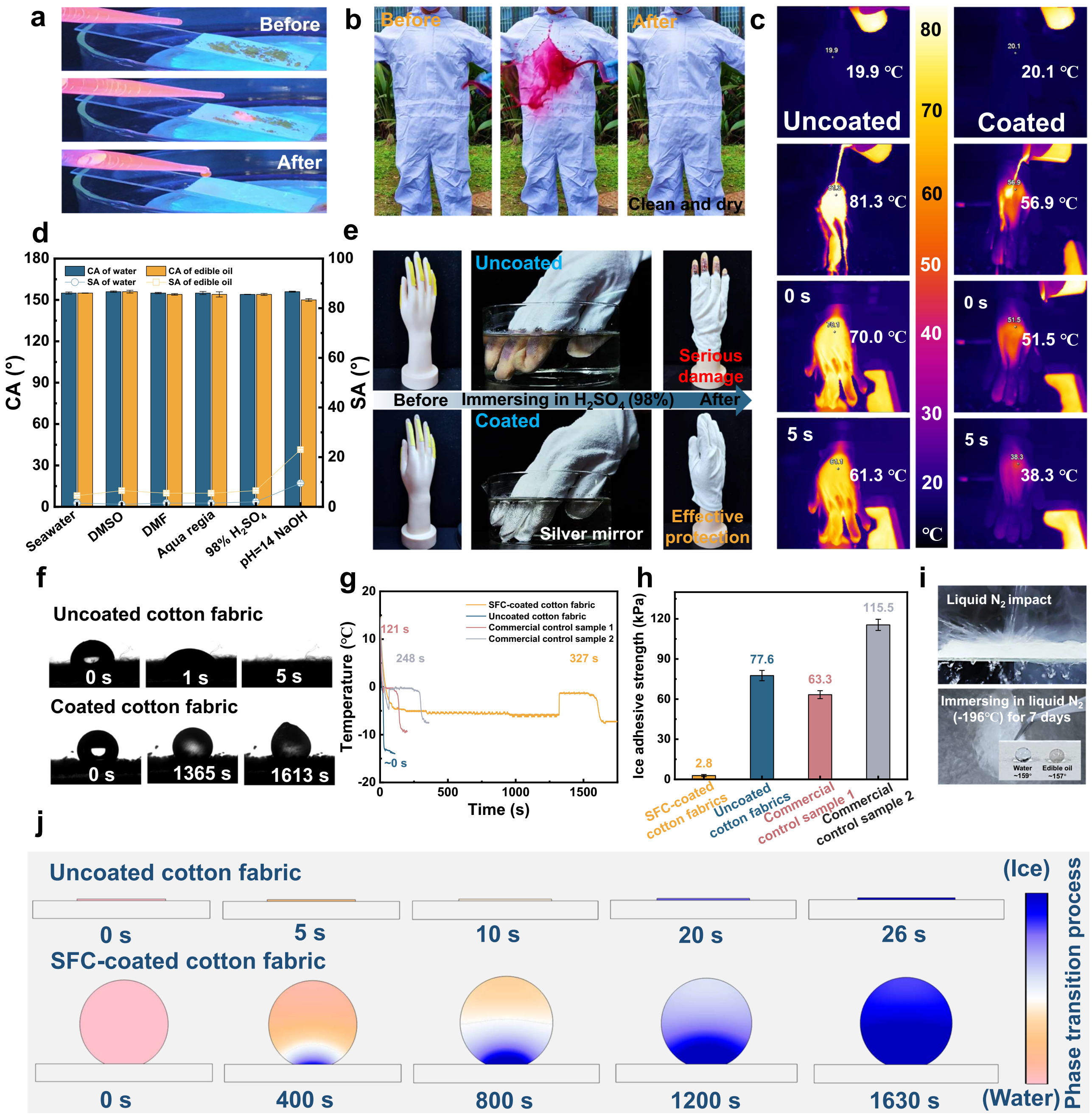

Fig. 4 | Antifouling, thermal liquid repulsion, cryogenic environment tolerance, and chemical corrosion resistance. a Self-cleaning test of the coated cotton fabric. **b** Antifouling test of the coated cotton protective clothing. **c** The temperature change of pouring boiling water (100 mL) on the uncoated and coated cotton gloves. **d** CAs and SAs of water and edible oil on the coated cotton after immersion in various solutions/solvents for 168 h. **e** Protection performance of uncoated and coated cotton gloves against concentrated H_2SO_4 (98%) for artificial hands (fingers wrapped in pH-indicator papers). **f** Freezing process (−15 °C) of water droplets (10 μL) on uncoated and coated cotton fabric. **g** Temperature-time curves for water on different surfaces during cooling. **h** Ice adhesion strength on different surfaces. **i** Digital photographs of pouring 50 mL of liquid N_2 onto the coated cotton fabric, along with the wettability of water and edible oil on the surface after 7 days of immersion in liquid N_2. **j** COMSOL simulations of the water droplet freezing process on the uncoated and SFC-coated cotton fabrics. The gradient scale represents the phase transition process from water to ice. All error bars represent the standard deviations calculated from at least three independent measurements. Source data are provided in the Source data file.

residue (Supplementary Fig. 30). In contrast, the coated cotton fabric can suppress flame spread after ignition and exhibits self-extinguishing behavior, leaving only a 9-cm char residue. The above results demonstrate that the coated cotton fabrics can effectively achieve a combination of excellent antifouling performance, thermal liquid repulsion, chemical corrosion resistance, cryogenic environment tolerance, and flame retardancy. This multifunctionality makes it a promising candidate for diverse applications, including personal protective equipment, advanced functional textiles, and outdoor products.

Durability, self-healing property and wear comfort

The durability and wear comfort of multifunctional fabrics are critical, particularly for applications such as personal protective clothing (Fig. 5a). Mechanical robustness of the coating is tested using Taber abrasion, sandpaper abrasion, washing, and tape-peeling tests. The

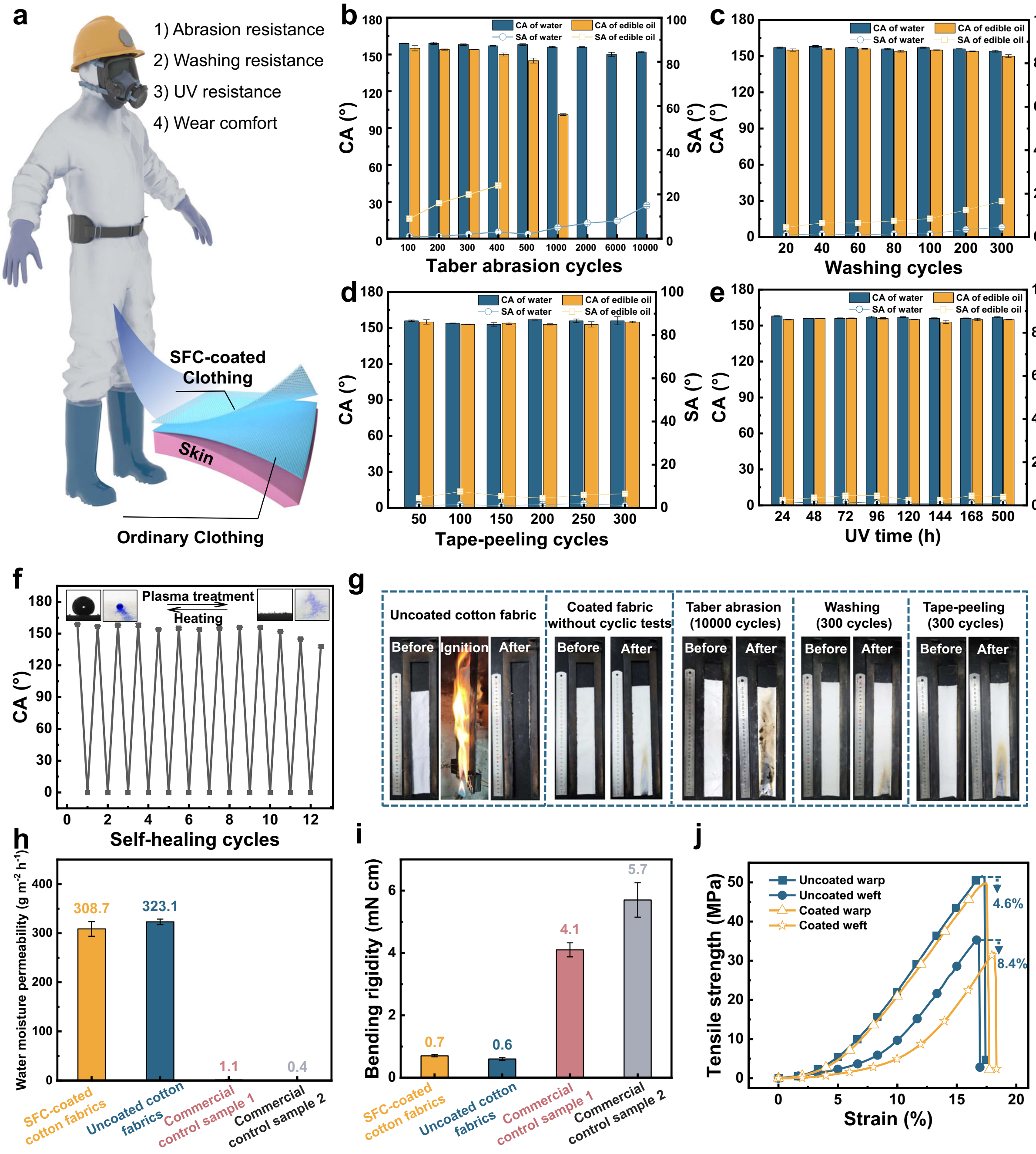

Fig. 5 | Durability, self-healing properties and wear comfort. **a** Schematic representation of SFC-coated fabrics applied in personal protective equipment. **b**–**e** CAs and SAs of water and edible oil on the coated cotton surface after cyclic Taber abrasion (**b**), washing (**c**), and tape-peeling tests (**d**). **e** CAs and SAs of water and edible oil on the coated cotton surface after UV-light irradiation test. **f** Water CAs on the surface of coated cotton fabric after multiple self-healing cycles. **g** Photographs of the as-prepared samples before and after the vertical burning tests. **h**–**j** Water moisture permeability (**h**), bending rigidity (**i**), and tensile strength (**j**) of the different samples. All error bars represent the standard deviations calculated from at least three independent measurements. Source data are provided in the Source data file.

coating can resist 400 cycles of Taber abrasion without losing its superamphiphobicity (Fig. 5b and Supplementary Fig. 31). Remarkably, the super-repellency of the coating can be well maintained even after 10,000 abrasion cycles. The declined oil repellency is primarily imputed to the damages of the nanostructures, while the microstructures remain sufficiently intact to preserve the superhydrophobicity. For comparison, the water CA of the coated surface without adhesive ($r = 1.0$) decreases to 138° after 2000 cycles (Supplementary Fig. 32). The SEM images further reveal that the coating is nearly completely destroyed, exposing the hydrophilic cotton fibers. Besides, the $r = 0.8$ sample can endure 2000 sandpaper abrasion cycles without losing its water repellency (Supplementary Fig. 33).

The coating also demonstrates excellent washing durability and tape-peeling resistance. After 300 cycles of washing and tape-peeling, the CAs of water and edible oil are still very high, and SEM images confirm the coating's integrity after washing and tape-peeling tests (Fig. 5c, d, Supplementary Figs. 34 and 35). These results manifest that the coating possess superior mechanical robustness, and the PDMS adhesive can enhance the coating durability by densely cross-linking the micro-protuberances and nanoparticles.

UV resistance tests show that the coated surfaces exhibit nearly unchanged wettability after 500 h of exposure to UV light (Fig. 5e and Supplementary Fig. 36), with surface morphology remaining well-preserved. Impressively, after 168 h of UV irradiation combined with 10,000 Taber abrasion cycles, the surface of the SFC-coated fabric still maintains its super-repellency, demonstrating its suitability for most outdoor applications in daily life (Supplementary Fig. 37).

Previous studies have demonstrated that endowing super-repellency surfaces with a self-healing property provides an effective way to enhance their durability[50]. The air plasma treatment can introduce hydrophilic oxygen-containing groups on the top layer of the coated fabric, similar to the effects of prolonged outdoor sunlight exposure in natural environments. After 100 s of plasma treatment, the coated fabric becomes superhydrophilic (Fig. 5f). However, the coating's liquid repellency is restored upon heating the chemically damaged fabric at 100 °C for approximately 2 h, with the water CA recovering to 157°. Figure 5f and Supplementary Fig. 38 demonstrate that this plasma/healing process can be repeated at least 10 times without diminishing the super-repellency or altering micro/nanostructures. The appreciable self-healing capability is primarily attributed to the healing agents PFDTES and PDMS (Supplementary Table 2). During the heating process, the internal perfluorinated chains and hydrophobic siloxane segments migrate to the surface, reducing surface energy and thus the declined super-repellency of the cotton fabric is repaired.

In practical applications, the durability of flame retardancy is equally essential. As demonstrated in Fig. 5g and Supplementary Fig. 39, after exposure to 10,000 Taber abrasion cycles, 300 washing cycles, 300 tape-peeling cycles, and 10 self-healing cycles, the add-on level of the coating on the fabrics shows a slight decrease. However, the coated fabrics can still self-extinguish immediately upon removal of the igniter during vertical burning tests, and their limiting oxygen index (LOI) values remain nearly unchanged. These results suggest the good durability of the coating, which is crucial for its long-term performance in maintaining flame retardancy.

In addition, the effects of the coating on the water moisture/air permeability, bending rigidity, and tensile strength of the cotton fabric are evaluated, as indicated in Fig. 5h–j and Supplementary Fig. 40. Compared to the uncoated fabric, the SFC-coated fabric retains approximately 95% of its water moisture permeability, 85% of its bending rigidity, and 90% of its tensile strength, ensuring satisfactory wear comfort. When compared to commercial control samples, the SFC-coated cotton fabrics offer significant multifunctional advantages, making them highly promising for advanced functional textiles and personal protective clothing applications (Supplementary Fig. 41).

Deformation-resistant performance

Superamphiphobic surfaces with deformation-resistant properties, essential for applications such as flexible smart devices and personal protective clothing, often lose liquid repellency under deformation due to the fragility of their rough structures. To address this, all-atom molecular dynamics (MD) simulations are conducted to assess the mechanical properties, and provide insights into strength and deformation resistance. During the simulated stretching process, the $r = 0.8$ sample with cross-linked PDMS can endure greater stress and strain compared to the $r = 1.0$ sample without cross-linking (Fig. 6a, b). The incorporation of PDMS significantly improves both strength and deformation resistance.

To study the surface wettability under different mechanical deformations, the $r = 0.8$ coating is applied to spandex, foam, and filter paper substrates. Both water and edible oil droplets maintain their spherical shape on the stretched coated spandex surface, even at a strain $\varepsilon = 200\%$ (Fig. 6c). Remarkably, after 10,000 cycles of stretching to $\varepsilon = 100\%$, the coated spandex surface remains superamphiphobic to both water and oil, with the coating uniformly covering the spandex surface (Fig. 6d and Supplementary Fig. 42). Although immersion in liquid N_2 temporarily reduces the spandex's stretchability, this property is fully restored at room temperature (Supplementary Fig. 43). Even after 7 days of immersion in liquid N_2 (Supplementary Fig. 44) or 500 h of UV exposure (Supplementary Fig. 45), the coated spandex retains its stretchable superamphiphobicity, demonstrating exceptional durability.

The coated foam also exhibits strong compression resistance (Fig. 6e). After 10,000 cycles of compression at $\varepsilon = 50\%$, the CAs for water and oil remain above 150°, with minimal surface changes (Fig. 6f and Supplementary Fig. 46). For bending deformation, the coated filter paper is bent into various shapes (Supplementary Fig. 47), yet water and oil droplets continue to bead on the surface (Fig. 6g). After 10,000 bending cycles at 180°, the anti-wetting properties of the surface remain nearly unchanged, and the coating's micro-nanostructures remain intact (Fig. 6h and Supplementary Fig. 48). These results indicate that the superamphiphobic coating exhibits strong deformation resistance under a variety of mechanical deformations.

To further understand the mechanism of the deformation resistance, the surface morphologies of the coated substrates are observed after stretching, compressing, and bending. The distances of fibers along the stretching direction increased with the strain increasing from 0% to 200%, while the distances of the fibers vertical to the stretching direction decreased (Supplementary Fig. 49). During compression, new protrusions formed on the foam surface as the strain increasing from 0% to 75% (Supplementary Fig. 50). As the bending angle increases, the apparent area of the coated filter paper gradually reduces (Supplementary Fig. 51). Despite these deformations, the SFC coating consistently maintains a tight connection with the substrates. This indicates that the observed changes in surface morphologies are primarily due to the substrate deformation, while the SFC coating adapts in tandem to preserve the monolithic macro-/micro-/nano hierarchical structure and stable superamphiphobicity.

In summary, we developed a deformation-resistant, superamphiphobic, and flame-retardant coating with exceptional environmental adaptability. By controlling the fraction of coating materials, a monolithic hierarchical macro-/micro-/nanostructure that exhibits remarkable superamphiphobicity is obtained, even after extensive deformation (including 10,000 cycles of stretching, compression, and bending). The stable air layer trapped by the coating results in an ultralow water adhesion force of only 0.002 mN, alongside impressive anti-fouling properties, thermal liquid repulsion at 100 °C, cryogenic resistance at −196 °C (liquid N_2), and chemical corrosion resistance (even against aqua regia and concentrated H_2SO_4). In addition, the coating imparts self-extinguishing behavior to flammable cotton fabric. The hydrogen bonding interactions and cross-linking adhesive enhance the coating's robustness by densely linking the micro protuberances and numerous nanoparticles, and thus the coated surfaces maintain nearly unchanged super-repellency even after 10,000 Taber abrasion cycles, 300 washing cycles, or 500 h of UV light irradiation. Compared to uncoated fabric, the coated materials retain about 95% of water moisture permeability, 85% of bending rigidity, and 90% of tensile strength. Owing to their multifunctionality and cost-effectiveness, these coatings show significant potential for applications in advanced functional textiles and personal protective clothing.

Methods

Materials

1H,1H,2H,2H-Perfluorodecyltriethoxysilane (PFDTES, 97%) was provided by J&K Scientific Co. Ltd. Silica nanoparticles (SiO_2, powders, ~15 nm in diameter), aluminum diethylphosphinate (ADP, phosphorus content: 23–24%) and tetraethyl orthosilicate (TEOS, 99%) were purchased from Aladdin Chemistry Co. Ltd. Polydimethylsiloxane (PDMS, Sylgard 184) was supplied by Dow Corning Corporation. Ethyl acetate (EA, 99.5%), ethanol (99.7%), glycerol (99%), n-hexadecane (98%), N,

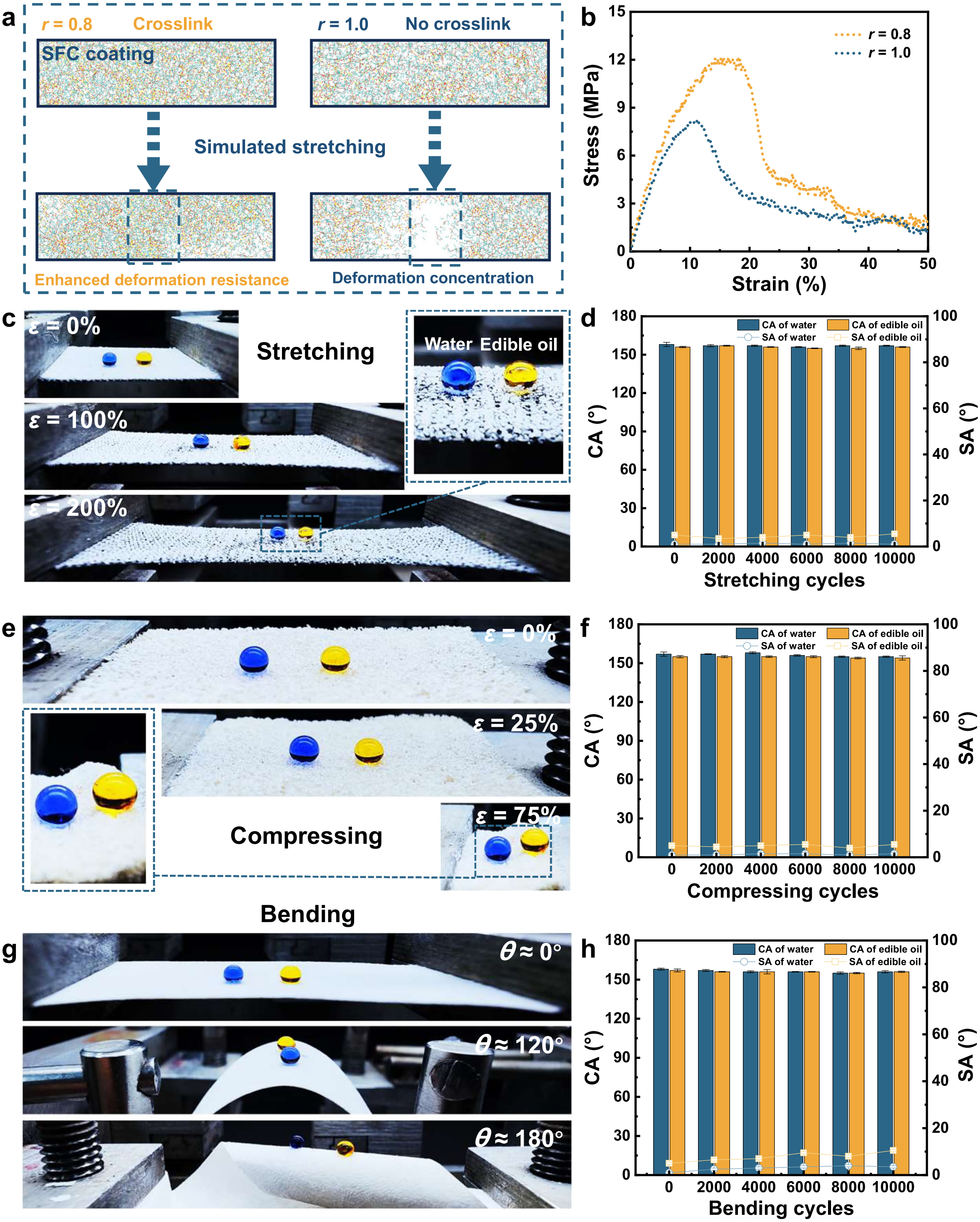

Fig. 6 | Deformation-resistant performance. **a** MD simulation snapshots for $r = 0.8$ coating with cross-linking and $r = 1.0$ coating without cross-linking at different stages of deformation. **b** Simulated stress-strain curves for the $r = 0.8$ and $r = 1.0$ coatings. **c**, **e**, **g** Digital photographs showing 10 μL droplets of water and edible oil on the surface of coated spandex under various strains (**c**), coated foam under different strains (**e**), and coated filter paper bent at various angles (**g**). $\varepsilon = (L_1 - L_0)/L_0 \times 100\%$, where L_0 is the original length of the substrate and L_1 is the stretched or compressed length. **d**, **f**, **h** The corresponding CAs and SAs of water and edible oil on the coated spandex after different stretching cycles ($\varepsilon = 100\%$) (**d**), coated foam after different compression cycles ($\varepsilon = 50\%$) (**f**) and coated filter paper after repeated bending cycles (180°) (**h**). All error bars represent the standard deviations calculated from at least three independent measurements. Source data are provided in the Source data file.

N-dimethylformamide (DMF, 99%), dimethyl sulfoxide (DMSO, 99%), rhodamine B (98%), methyl blue (95%), amaranth (85%), concentrated HCl (36–38%), concentrated HNO_3 (65–68%), concentrated H_2SO_4 (95–98%), NaOH (98%) and ammonia (25–28%) were obtained from Kelong Chemical Industrial Reagent Co. The seawater was collected from the Yellow Sea (Tsingtao, China). Commercial cotton fabric ($132 \pm 3\,g\,m^{-2}$), spandex fabric ($100 \pm 2\,g\,m^{-2}$), chemical protective clothing (Tychem C, Dupont, USA), firefighting clothing (Tianjin Fire Science and Technology Research Institute of Ministry of Emergency Management, China), polyurethane foam, filter paper, rubber hands, edible oil, diesel oil, milk and coffee were purchased from a local supermarket. Unless otherwise specified, all reagents and solvents were of analytical grade and used without further purification.

Preparation of F-SiO_2 nanoparticles

F-SiO_2 was prepared with the modified Stöber method. SiO_2 (1.0 g, ~16.6 mmol) was dispersed in ethanol (50 mL), followed by injection of TEOS (2 mL, ~8.96 mmol) and ammonia (10 mL). Subsequently, PFDTES (1 mL, ~2.96 mmol) was added to the solution under stirring for 6 h at room temperature. The F-SiO_2 was centrifuged, washed three times with EA, and dried at 80 °C for 12 h, yielding approximately 1.6 g of product.

Fabrication of the SFC coatings

The fabrication process of SFC is as follows: First, PDMS (1.0 g) was mixed with a curing agent in a weight ratio of 10:1 and dissolved in EA (50 mL). Then, F-SiO_2 (2.0 g), ADP (2.0 g), and PFDTES (1.0 mL) were added in the above solution to fabricate SFC suspensions by magnetic stirring for 3 h. After that, the superamphiphobic surfaces were prepared by spraying the suspension onto substrates (such as glass, cotton fabric, spandex fabric, form, and filter paper) with a W-101G spray gun (1.0 mm of nozzle orifice; 0.3 MPa of pressure; $5\,cm\,s^{-1}$ of moving rate). The spray gun was held 10 cm from the fabric and moved in an S-pattern to ensure uniform spraying. The add-on level and coating thickness were controlled by adjusting the volume of the coating solution. The add-on level ($g\,m^{-2}$) of the coatings was then calculated using Eq. (1):

$$\text{add} - \text{on} = \frac{m_1 - m_0}{A_0} \times 100\% \tag{1}$$

where m_0 and m_1 represent the weight of the samples before and after coating, respectively, and A_0 is the surface area of the samples.

The SFC coating solutions were prepared using different mass ratios of F-SiO_2, ADP, and PDMS. The total mass was kept constant, with the mass ratio (r) of micro-/nano-particles regulated according to the Eq. (2):

$$r = \frac{W_{F-SiO2} + W_{ADP}}{W_{F-SiO2} + W_{ADP} + W_{PDMS}} \tag{2}$$

where W represents the weight of the components. Furthermore, with a fixed r-value, the ratio between F-SiO_2 and ADP is adjusted. More detailed data are provided in Supplementary Tables 3 and 4.

The additional experimental information including characterization, mechanical stability and UV resistance, chemical stability, anti-icing performance, quantum chemistry calculation, all-atom molecular dynamics simulation and finite element methods simulation is available in the Supplementary Information. All procedures were performed in accordance with standard laboratory safety protocols to eliminate potential hazards associated with the reagents and reactions.

Data availability

The data supporting the findings of the study are included in the main text and supplementary information files. Raw data can be obtained from the corresponding author upon request. Source data are provided with this paper.

References

1. He, H.-L. et al. An utralight self-powered fire alarm e-textile based on conductive aerogel fiber with repeatable temperature monitoring performance used in firefighting clothing. *ACS Nano* **16**, 2953–2967 (2022).
2. Xu, Y.-J. et al. Research progress on flame-retardant and muti-functionalization of textiles. *J. Text. Res.* **43**, 1–9 (2022).
3. Liu, B.-W., Zhao, H.-B. & Wang, Y.-Z. Advanced flame-retardant methods for polymeric materials. *Adv. Mater.* **34**, 2107905 (2022).
4. Lazar, S. T., Kolibaba, T. J. & Grunlan, J. C. Flame-retardant surface treatments. *Nat. Rev. Mater.* **5**, 259–275 (2020).
5. Li, J.-L. et al. A top-down and in situ strategy for intrinsic acicular nanostructure enhanced ultradurable superhydrophobic and anti-icing aramid fabric. *Chem. Eng. J.* **484**, 149569 (2024).
6. Mao, L.-Z. et al. Crocodile skin-inspired protective composite textiles with pattern-controllable soft-rigid unified structures. *Adv. Funct. Mater.* **33**, 2213419 (2023).
7. Tao, Y. et al. Cotton/alginate blended knitted fabrics: flame retardancy, flame-retardant mechanism, water absorption and mechanical properties. *Cellulose* **28**, 4495–4510 (2021).
8. Qi, P. et al. Ultra washing durable flame retardant coating for cotton fabric by the covalent bonding and interface polymerization. *Chem. Eng. J.* **452**, 139453 (2023).
9. Wang, F. et al. A four-tier hierarchical architecture for super-amphiphobic and flame-retardant fabrics with enhanced self-buoyancy and anti-icing properties. *Chem. Eng. J.* **488**, 151084 (2024).
10. Wang, F. et al. Superamphiphobic and flame-retardant coatings with highly chemical and mechanical robustness. *Chem. Eng. J.* **421**, 127793 (2021).
11. Ma, Z.-W. et al. A lava-inspired micro/nano-structured ceramifiable organic-inorganic hybrid fire-extinguishing coating. *Matter* **5**, 911–932 (2022).
12. Song, J.-N. et al. Durable radiative cooling against environmental aging. *Nat. Commun.* **13**, 4805 (2022).
13. Li, P. et al. Ecofriendly flame-retardant cotton fabrics: preparation, flame retardancy, thermal degradation properties, and mechanism. *ACS Sustain. Chem. Eng.* **7**, 19246–19256 (2019).
14. Pan, Y., Liu, L.-X., Wang, X., Song, L. & Hu, Y. Hypophosphorous acid cross-linked layer-by-layer assembly of green polyelectrolytes on polyester-cotton blend fabrics for durable flame-retardant treatment. *Carbohydr. Polym.* **201**, 1–8 (2018).
15. Lin, D.-M., Zeng, X.-R., Li, H.-Q., Lai, X.-J. & Wu, T.-Y. One-pot fabrication of superhydrophobic and flame-retardant coatings on cotton fabrics via sol-gel reaction. *J. Colloid Interface Sci.* **533**, 198–206 (2019).
16. Chen, S.-S., Li, X., Li, Y. & Sun, J.-Q. Intumescent flame-retardant and self-healing superhydrophobic coatings on cotton fabric. *ACS Nano* **9**, 4070–4076 (2015).
17. Wang, X.-Y. et al. Durable fire retardant, superhydrophobic, abrasive resistant and air/UV stable coatings. *J. Colloid Interface Sci.* **582**, 301–311 (2021).
18. Sun, R.-Y. et al. Formulation of environmentally robust flame-retardant and superhydrophobic coatings for wood materials. *Constr. Build. Mater.* **392**, 131873 (2023).
19. Li, C.-B. et al. A multifunctional coating towards super-hydrophobicity, flame retardancy and antibacterial performances. *Chem. Eng. J.* **450**, 138031 (2022).
20. Ma, Z.-W. et al. Bioinspired, highly adhesive, nanostructured polymeric coatings for superhydrophobic fire-extinguishing thermal insulation foam. *ACS Nano* **15**, 11667–11680 (2021).

21. Zhang, C.-Y. et al. Shelter forest inspired superhydrophobic flame-retardant composite with root-soil interlocked micro/nanostructure enhanced mechanical, physical, and chemical durability. *Adv. Funct. Mater.* **33**, 2213398 (2023).
22. Wang, F. et al. A superhydrophobic coating to create multi-functional materials with mechanical/chemical/physical robustness. *Chem. Eng. J.* **381**, 122539 (2020).
23. Wang, D.-H. et al. Design of robust superhydrophobic surfaces. *Nature* **582**, 55–59 (2020).
24. Peng, C.-Y., Chen, Z.-Y. & Tiwari, M. K. All-organic superhydrophobic coatings with mechanochemical robustness and liquid impalement resistance. *Nat. Mater.* **17**, 355–360 (2018).
25. Wong, W. S. Y. Surface chemistry enhancements for the tunable super-liquid repellency of low-surface-tension liquids. *Nano Lett.* **19**, 1892–1901 (2019).
26. Wu, B.-R. et al. Porous bulk superhydrophobic nanocomposites for extreme environments. *Matter* **6**, 1992–2004 (2023).
27. Gu, W.-C. et al. Ultra-durable superhydrophobic cellular coatings. *Nat. Commun.* **14**, 5953 (2023).
28. Liu, L.-Y. et al. Transparent self-cleaning coatings repellent to ultralow surface tension liquids in extreme environments. *Chem. Eng. J.* **482**, 148921 (2024).
29. Pei, L.-C. et al. A multifunctional and long-term waterborne anti-corrosion coating with excellent 'hexagonal warrior' properties. *Chem. Eng. J.* **457**, 141158 (2023).
30. Zhang, H.-L. et al. A skin-inspired design integrating mechano–chemical–thermal robustness into superhydrophobic coatings. *Adv. Mater.* **34**, 2203792 (2022).
31. Zang, X.-R. et al. A robust biomimetic superhydrophobic coating with superior mechanical durability and chemical stability for inner pipeline protection. *Adv. Sci.* **11**, 2305839 (2024).
32. Li, H.-J. et al. Transparent superamphiphobic material formed by hierarchical nano re-entrant structure. *Adv. Funct. Mater.* **34**, 2309684 (2024).
33. Wei, J.-F. et al. Scalable robust superamphiphobic coatings enabled by self-similar structure, protective micro-skeleton, and adhesive for practical anti-icing of high-voltage transmission tower. *Adv. Funct. Mater.* **32**, 2206014 (2022).
34. Li, Z. et al. Surface-embedding of functional micro-/nanoparticles for achieving versatile superhydrophobic interfaces. *Matter* **1**, 661–673 (2019).
35. Zhou, X.-T., Liu, J., Liu, W.-D., Steffen, W. & Butt, H.-J. Fabrication of stretchable superamphiphobic surfaces with deformation-induced rearrangeable structures. *Adv. Mater.* **34**, 2107901 (2022).
36. Pan, S.-J. et al. Coatings super-repellent to ultralow surface tension liquids. *Nat. Mater.* **17**, 1040–1047 (2018).
37. Zhang, J.-H. et al. Fabrication and energy collection of superhydrophobic ultra-stretchable film. *Adv. Funct. Mater.* **34**, 2400024 (2024).
38. Dong, J.-C. et al. Ultra-stretchable and superhydrophobic textile-based bioelectrodes for robust self-cleaning and personal health monitoring. *Nano Energy* **97**, 107160 (2022).
39. Wei, J.-F. et al. Durable superhydrophobic coatings for prevention of rain attenuation of 5 g/weather radomes. *Nat. Commun.* **14**, 2862 (2023).
40. Wang, S.-L. et al. Superdurable full-life superhydrophobic composite block. *Adv. Mater.* **36**, 2403853 (2024).
41. Liu, L.-M. et al. Anti-/deicing membranes with damage detection and fast healing. *Adv. Funct. Mater.* **n/a**, 2404760 (2024).
42. Kim, H., Lee, Y.-J., Jung, S. & Lee, H. Micropatterned hydrogel-elastomer hybrids for flexible wet-style superhydrophobic anti-fogging tapes. *Adv. Funct. Mater.* **34**, 2401869 (2024).
43. Tesler, A. B. et al. Long-term stability of aerophilic metallic surfaces underwater. *Nat. Mater.* **22**, 1548–1555 (2023).
44. Udayraj, Talukdar, P., Das, A. & Alagirusamy, R. Heat and mass transfer through thermal protective clothing—a review. *Int. J. Therm. Sci.* **106**, 32–56 (2016).
45. Zhang, J.-Y. et al. A biomimetic closed-loop recyclable, long-term durable, extreme-condition resistant, flame-retardant nanocoating synthesized by reversible flocculation assembly. *Mater. Horiz.* **10**, 4551–4561 (2023).
46. Chen, J.-Y. et al. Ultra-highly stiff and tough shape memory polyurea with unprecedented energy density by precise slight cross-linking. *Adv. Mater.* **36**, 2401178 (2024).
47. Zhao, Z.-M., Li, P.-F., Li, Y.-C. & Wang, S.-L. Durable thermal fluid super-repellency of elastic fluorine-modified sio2@sponge composite aerogel. *Chem. Eng. J.* **454**, 140247 (2023).
48. Tian, N., Chen, K., Wei, J.-F. & Zhang, J.-P. Robust superamphiphobic fabrics with excellent hot liquid repellency and hot water vapor resistance. *Langmuir* **38**, 5891–5899 (2022).
49. Li, W.-L. et al. In situ growth of a stable metal–organic framework (MOF) on flexible fabric via a layer-by-layer strategy for versatile applications. *ACS Nano* **16**, 14779–14791 (2022).
50. Zhou, H., Niu, H.-T., Wang, H.-X. & Lin, T. Self-healing superwetting surfaces, their fabrications, and properties. *Chem. Rev.* **123**, 663–700 (2023).

Acknowledgements

This work was supported by the National Key R & D Program of China (2022YFB3806401 to F.W.), the National Natural Science Foundation of China (52203274 to F.W.), the Fundamental Research Funds for the Central Universities, the "111 Center" (B20001 to Y.-Z.W.), and Institutional Research Fund from Sichuan University (2021SCUNL201 to X.-L.W.). We also gratefully acknowledge Professor Xiu-Li Wang for her support with funding and resources.

Author contributions

F.W. and Y.-Z.W. conceived and directed the research. C.-B.L. and F.W designed and performed the experiments. Y.-Y.W., M.-L.G., and J.-L.L. assisted with durability measurement. C.D., F.S., and W.Y. participated in data interpretation and discussion. C.-B.L. wrote the initial manuscript draft. F.W. edited the draft. All authors contributed to the revised manuscript.

Competing interests

The authors declare no competing interests.

Additional information

Supplementary information The online version contains supplementary material available at https://doi.org/10.1038/s41467-025-58191-w.

Correspondence and requests for materials should be addressed to Fang Wang or Yu-Zhong Wang.

Peer review information *Nature Communications* thanks the anonymous reviewers for their contribution to the peer review of this work. A peer review file is available.